Journal of Materials Chemistry A

Accepted Manuscript

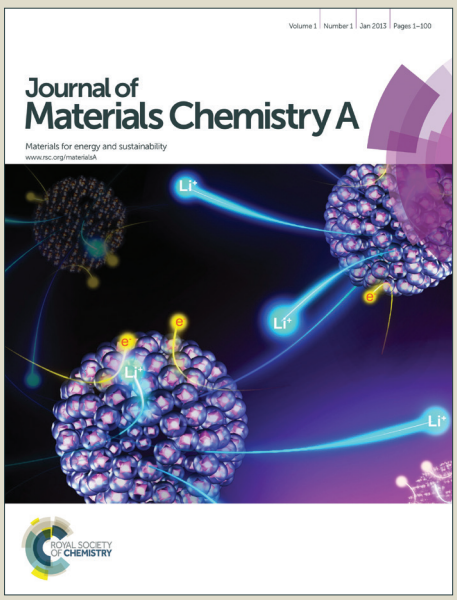

ROYAL SOCIETY OF CHEMISTRY

www.rsc.org/materialsA

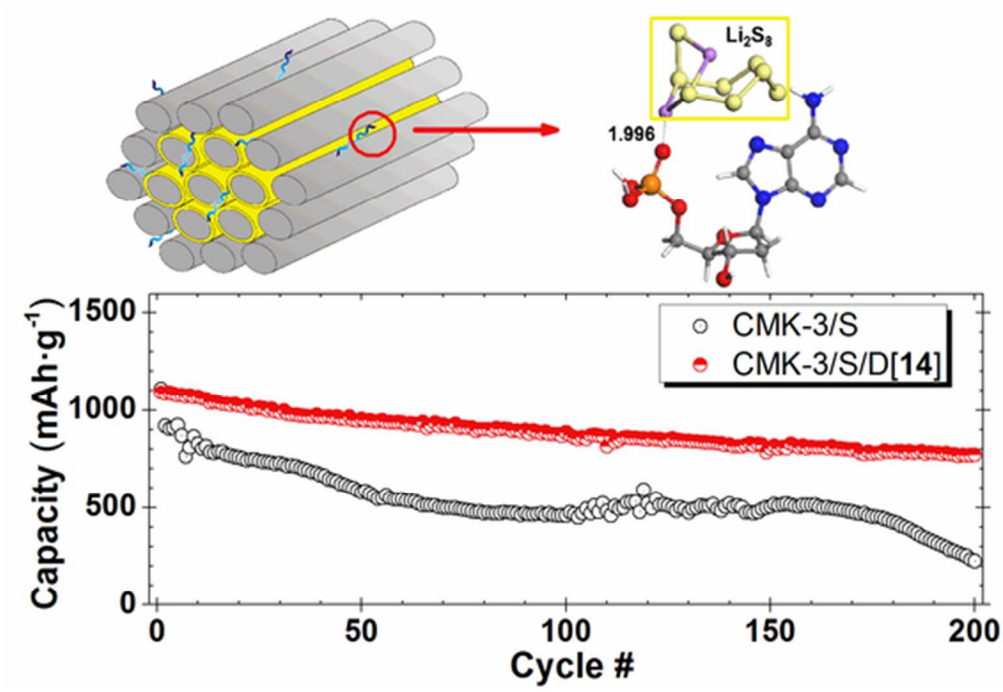

Fine amount of DNA incorporated CMK-3/S cathodes could anchor soluble polysulfides for considerably improving the cycling performance of Li/S batteries.
47x32mm (300 x 300 DPI)

Journal of Materials Chemistry A

RSCPublishing

ARTICLE

High-Performance Lithium/Sulfur Batteries by Decorating CMK-3/S with Fine-amount DNA

Cite this: DOI: 10.1039/x0xx00000x

Qiyang Li[a], Chenggang Zhou[a*], Zhuan Ji[a], Bo Han[a], Liang Feng[b] and Jinping Wu[a*]

Received 00th January 2015,
Accepted 00th January 2015

DOI: 10.1039/x0xx00000x

www.rsc.org/

Prohibiting lithium polysulfides from being dissolved to electrolyte is the most critical challenge for pursuing high-performance Li/S battery. Taking full advantage of interactions between polysulfides and functional groups of third-party additives has been proven to be an efficient strategy. In the present work, we selected DNA to decorate the CMK-3/S cathodes. The −P=O and =N− sites of the constituent deoxyribonucleotides of DNA are demonstrated to be capable of anchoring polysulfides through our DFT calculations. Experimental results show that a fine adding amount of DNA into the CMK-3/S composite enables a significant improvement to cyclic performance. In particular, with a moderate DNA loading rate, the DNA post-load procedure offers a discharge capacity of 771 mAh·g^{-1} at 0.1 C after 200 cycles (retention 70.7% of the initial), which behaves slightly better than the DNA pre-load procedure. The proposed DNA decorating scheme may provide an applicable technical solution for developing high-performance Li/S batteries for fulfilling market.

Introduction

Rechargeable lithium/sulfur battery promises an appealing candidate for energy storage to power portable devices and electric vehicles. However, sulfur electrode encounters several vital intrinsic disadvantages, including low conductivity, volume expansion during discharge and dissolution of polysulfides to organic electrolyte. In particular, the shuttle-effect resulted from severe dissolution of polysulfides leads to low active materials utilization, low Coulombic efficiency and unaffordable performance decay, which inhibits the Li/S cells from being practically deployed.

In recent years, many strategies[1-6] have been attempted to confront these challenges, especially the polysulfides dissolution problem. Most efforts have been focused on cathode assembly and modification. Employing ordered carbons, involving carbon nanotubes[7-10], graphene[11-21], ordered mesoporous carbon[22-24], hollow carbon sphere[25, 26], nanofiber[27, 28] and microporous carbon sphere[29, 30], instead of active carbon as conductive substrate have become a prevalent trend. For S content stored in the ordered pores of carbon, the polysulfide dissolution should be significantly lowered down due to the limited opening edges of the pores, leading to a higher S uptake as well as enhanced cyclic performance can be achieved. Unfortunately, the current S uploading techniques, either melting-diffusion or chemical-deposition, are not able to guarantee that all S contents are stored inside the meso- or micro-pores, instead, partial S residing outside the pores will be rapidly lost. On the other aspect, polysulfide dissolving from the opening edge of the pores should not be substantially forbidden. Wrapping S in conductive polymers within core-shell structure such as S@PPy[31-33], S@PANI[34, 35], S@PVP[36] and S@PEDOT[37, 38], can provide a full protection for isolating polysulfides from electrolyte. However, the poor conductivity of conductive polymers would increase the internal resistance of the cell.

Hybridizing the C/S composite with third-party coatings, including polymers polymers[22, 28, 39-48] or oxides[49-51], has become another focal point for further improving the performance of C/S cathodes. Polymers are generally coated on the C/S complexes, i.e., Nazar et al[22] proved that the discharge capacity of polyethylene glycol (PEG) modified CMK-3/S (PEG@CMK-3/S) is considerably higher than original CMK-3/S by 300 mAh·g^{-1}; similar systems, such as PEDOT-PSS@CMK-3/S[28], and PVP@hollow carbon nanofiber[39] reported by Cui et al, PANI@C/S reported by Gao et al[42] and PPy@CMK-8/S reported by Wen et al[48], have also been demonstrated to own superior performance than unmodified C/S electrodes. In contrast, oxide coating has two executive procedures. Nazar et al[49] utilized MO_x (SiO_x and VO_x) to

encapsulate CMK-3/S. The SiO_x@CMK-3/S cathode exhibits a reversible capacity of 718 mAh·g^{-1} and sustains up to 82.5% of initial capacity after 60 cycles. Cui et al[50] prepared the yolk-shell structure TiO_2@S and then incorporate with Super P. At a rate of 0.5 C, the initial cycle capacity is 1030 mAh·g^{-1} which decays only 0.033% per cycle within 1000 cycles. Recently, Nazar et al[52] developed the Ti_4O_7/S cathode materials which also enabled very stable cycling performances within 500 cycles.

The modification implemented by these third-party agents, in most cases, isolates S contents from electrolyte. Many studies suggested that the retarding of polysulfide dissolution can also be attributed to the polysulfide adsorption on the functional groups of third-party agents, such as -NH_x in PPy and PANI[24, 28, 33-36, 40], ether groups in PEDOT and PEG[22, 28], and hydroxyl groups on oxide surfaces[49]. Not coincidentally, N-doping of the conductive carbons, as reported by Song et al[53] and Zhang et al[54], could improve the interactions between the oxygen functional groups in the carbon substrate and the polysulfides. Of course, these 'sulphiphilic' interactions[52], implemented by functional groups of either self-contained or third-party agents, should be capable of anchoring lithium polysulfides to slow down dissolution, as suggested by theoretical calculations conducted by Cui et al[55]. It is not difficult to envision that, for those efforts, the relatively large loading amount of third-party agents, either polymers or oxides, implies not only higher internal resistance but capacity penalty. Enlarging the anchoring role of third-party additives brought by the interactions hereby becomes a promising approach. To balance the energy density and the polysulfide adsorption, the candidate agents should be light-weighted, rich of functional groups and can be easily dispersed homogeneously in the C/S composite.

Based on these understanding, we selected DNA as a model additive to conduct the proof-of-concept studies. DNA strains own high concentration of heteroatoms including O, N, and P, which may serve as absorbent for anchoring polysulfides. Upon integration with certain substrate which allows a well-dispersion of DNA, the quasi-linear structure of DNA implies that the heteroatoms are mostly disposed to the target adsorbates, which should maximize the anchoring function. In the present work, we demonstrated that introducing a fine amount of DNA into the C/S cathode materials enables a considerable performance improvement.

Results and discussion

We first performed first-principles density functional theory calculations on the adsorption behaviours of polysulfides on DNA strains. To simplify the calculation, we employed the four deoxyribonucleotides (namely A, T, G and C) to represent DNA strains. Li_2S_8, which has been recognized as the most soluble polysulfide[56], was selected as the probe molecule to investigate the interaction configurations and energetics. The calculated adsorption energies on different sites of the deoxyribonucleotides are listed in Table 1, while the computational details as well as the adsorption structures (Fig. S1) are included in the supporting information. As suggested by Cui et al[55], the electron-enriched groups are affinitive to the Li^+ ions, which exhibit as −P=O, −C=O, −OH, =N−, $-NH_2$ and –NH− groups in A, T, G and C in the selected substrate. The data in Table 1 show that Li_2S_8 adsorptions show very weak dependence on the type of deoxyribonucleotides, however, prefer to attach on the −P=O and =N− sites which possess the strongest adsorption strength of higher than 0.9 eV per molecule, much higher than other candidate sites. The calculated energies are comparable to the previous report[55], which have demonstrated that polysulfide dissolution can be retarded upon such an interaction. The data validate our expectation that DNA is capable of anchoring polysulfides.

Table 1. The calculated adsorption energies (E_{ads}) on different sites of the deoxyribonucleotides (A, T, G and C)

E_{ads}(eV)	−P=O	−C=O	−OH	=N−	$-NH_2$	−NH
A	1.077	--	0.485	1.068	0.381	--
T	1.044	0.656	0.460	--	--	0.108
G	1.095	0.861	0.467	0.992	0.182	0.097
C	1.089	0.864	0.515	0.911	0.411	--

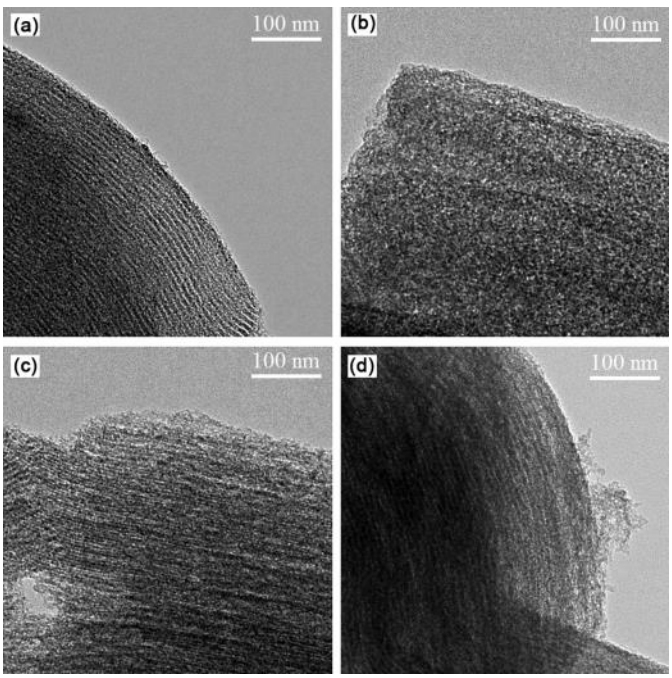

Figure 1. TEM images of (a) bare CMK-3, (b) CMK-3/S, (c) CMK-3/D[**14**]/S and (d) CMK-3/S/D[**14**].

Figure 1 shows the TEM morphologies of bare CMK-3 substrate, CMK-3/S, CMK-3/D[**14**]/S and CMK-3/S/D[**14**] samples, respectively. The sequence of the abbreviation for the latter two samples represents the loading order of DNA and S, while the number in the square brackets denotes that the DNA loading rate was set to be 14 mg·g^{-1} S. Detailed descriptions can be found in the experimental section. The thermal stability of pure DNA and the S uptake were examined via the

simultaneous TG-DSC measurement (Fig. S2-S4 and Table S1), while the BJH characterization results (Fig. S5) are summarized in Table S2. Within the temperature range of 30-155 ℃, the only weight loss of DNA originates from the absorbed water which accounts for 4.2 wt% below 100 ℃. Above 100 ℃, both TG and DSC curves level out, suggesting that DNA would not decompose in our melting-diffusion procedure. Table S1 indicates that, with a designated DNA loading (14 mg·g^{-1} S for both pre- and post-load cases), the average S content of the three types of samples are all measured to be around 56.0 wt%. Upon S impregnation as well as DNA pre- or post-incorporation, both the BET specific surface area and the total pore volume shrink significantly (Fig. S5 and Table S2), suggesting that most mesopores of CMK-3 have been occupied by S. However, the participation of DNA in the cathode materials, either pre- or post-load, results in only slight variation to the BJH mesopore features. For CMK-3, such a loading rate (below than the theoretical value of 70 wt%) promises sufficient expansion space to accommodate the lithium polysulfides at discharge[22], while, the micro morphology were kept intact in our preparation procedures, as demonstrated by the TEM and SEM characterizations shown in Fig. 1 and Fig. S6, respectively.

The charge/discharge performance of the DNA decorated CMK-3/S test cells as well as bare CMK-3/S test cells at 0.1 C (1 C=1675 mA·g^{-1}) are depicted in Fig. 2(a) and 2(b). For the pre-load series (Fig. 2(a)), the cyclic performance depends heavily with DNA loading rate and, in particular, the first discharge capacity decreases with the increasing DNA loading for the DNA-engaged cathodes. At a medium DNA loading rate, a first discharge capacity of 1150 mAh·g^{-1} (all of the specific capacities were calculated by sulfur mass) was achieved, with an optimal capacity retention of 76.5% after 100 cycles and 64.4% after 200 cycles at 0.1 C (fading rate of 0.178%), which is considerably improved comparing with raw CMK-3/S (initial capacity of 1109 mAh·g^{-1} , retention rate of 41.3% after 100 cycles and 20.3% after 200 cycles at same discharge condition, comparable to reported performances[22, 48]). In comparison, for lower (CMK-3/D[**7**]/S) or higher (CMK-3/D[**22**]/S) DNA loading, rapid capacity decay were observed in incipient 40 cycles. Despite the difference for the two initial discharge capacity, low DNA loading behave better than high loading. For long-term discharge, these two samples have approximate performance with CMK-3/S electrodes.

Unlike the pre-load cases, the DNA post-load samples exhibit much weaker dependence between capacity retention and DNA loading rate. Although the first discharge capacities vary with the DNA loading rate, again, a medium DNA loading (CMK-3/S/D[**14**]) gives the best cyclic performance with the retention rate of 81.1% and the capacity remains 884 mAh·g^{-1} after 100 cycles, which is approximate to that of CMK-3/D[**14**]/S at 0.1 C, while, slightly higher than CMK-3/D[**14**]/S after 200 cycles (771 mAh·g^{-1} vs. 741 mAh·g^{-1}, fading rate of 0.116% vs. 0.178% per cycle). Considering the fact that the initial discharge capacity of CMK-3/D[**14**]/S is higher than CMK-3/S/D[**14**], we can conclude that the post-load procedure has a more stable cyclic performance than pre-load cases for long-term discharging. For lower (7 mg·g^{-1}) and higher (22 mg·g^{-1}) DNA loading, the discharging behaviours are similar to the curve of CMK-3/S/D[**14**], while behave much better than that of the pre-load cases for the same DNA loading rates (43.6% vs. 27.4% for 7 mg·g^{-1} S, and 52.8% vs. 37.4% for 22 mg·g^{-1} S after 200 cycles, respectively).

The two optimal samples with moderate DNA loading, CMK-3/D[**14**]/S and CMK-3/S/D[**14**], were successively selected to investigate their C-rate performance as presented in Fig. 2(c) and 2(d). The retention rate of CMK-3/D[**14**]/S at 0.2 C exhibits approximate behaviour as what was observed for 0.1 C. While at 0.5 C, not only the initial discharge capacity is 200 mAh·g^{-1} lower than the above two rates, but the discharge capacity encounters a linear drop down with respect to the cycle number. In contrast, the capacity retention behaviour of CMK-3/S/D[**14**] has a nonnegligible dependence to the discharge rate.

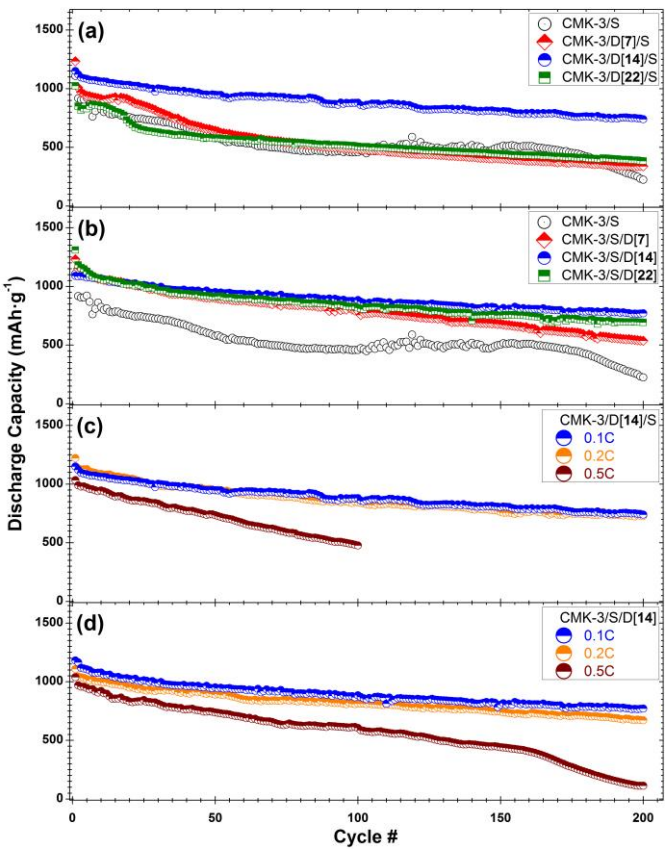

Figure 2. The discharge capacity for 200 charge/discharge cycles of (a). DNA Pre-load samples at 0.1 C; (b). DNA post-load samples at 0.1 C; (c). CMK-3/D[**14**]/S at 0.1 C, 0.2 C and 0.5 C; and (d). CMK-3/S/D[**14**] at 0.1 C, 0.2 C and 0.5 C. The discharge behaviour of CMK-3/S is also included in (a) and (b) for purpose of comparison.

At 0.5 C, the capacity decays sharply from 1039 mAh·g^{-1} to 606 mAh·g^{-1} after 100 cycles, which is better than that of CMK-3/D[**14**]/S (1034 mAh·g^{-1} to 477 mAh·g^{-1}, 58.3% vs.

46.1%). The results indicate that the DNA modification might not be suitable for high-rate discharge.

From the discharge-charge profiles of the two optimal samples (CMK-3/D[**14**]/S and CMK-3/S/D[**14**]) depicted in Fig. 3, we observed that at low rate (0.1 C), both two sample have typical secondary plateau at 2.1 V after 200 cycles, suggesting that the polysulfides are strongly attached on the electrode instead of dissolution, as evidenced by the behaviour of undecorated CMK-3/S. At moderate rate (0.2 C), the secondary plateau of CMK-3/S/D[**14**] acts slightly stable than CMK-3/D[**14**]/S. Although the cyclic performance of pre-load samples are slightly weaker than that of post-load at low and moderate C-rate, however, the Coulombic efficiency exhibits reverse trend (~86% of pre-load vs. ~76% of post-load) in Fig. S7. At higher rate (0.5 C), the diminished plateau suggests that electrochemical polarization become severe due to the increasing current rate.

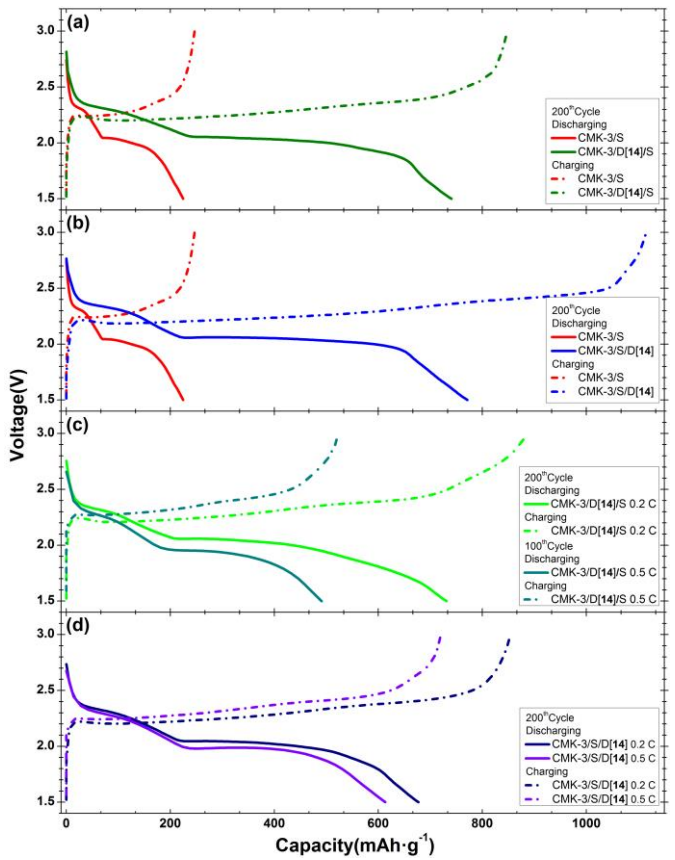

Figure 3. Discharge-charge profiles of (a). CMK-3/D[**14**]/S at 0.1C (200th); (b). CMK-3/S/D[**14**] at 0.1 C (200th); (c). CMK-3/D[**14**]/S at 0.2 C (200th) and 0.5 C (100th); and(d). CMK-3/S/D[**14**] at 0.2 C (200th) and 0.5 C (100th). The discharge-charge profiles of CMK-3/S are also included in (a) and (b) for purpose of comparison.

We next collected the Nyquist plots of fresh and discharged CMK-3/S, CMK-3/D[**14**]/S and CMK-3/S/D[**14**] test cells as displayed in Fig. 4. Using the equivalent circuit[57, 58] shown in inset, the plots agree well with the collected impedance spectra and the detailed element values are listed in Table S3. R_{el} represents the Ohmic resistances of electrolyte and electrode. For fresh cells, R_{el} varies very slightly for pre-load, while increases almost linearly with DNA loading for post-load. The C_{sl}//R_{sl} and CPE_1//R_{er} elements in the equivalent circuit denote the impedance of surface layer and electrochemical reaction, respectively. We used the CPE elements instead of capacitor units since the porous materials can hardly exhibit ideal capacitor behaviour. For fresh cathodes, all elements, except R_{er}, behave approximately. Upon long-term charge/discharge, the impedances of CMK-3/S change considerably comparing with fresh electrode, as indicated by the sharp increase of R_{el}, which should be caused by the deposition of inert Li_2S on the electrode surface and the dissolution of polysulfides. For CMK-3/D[**14**]/S and CMK-3/S/D[**14**], R_{el} changes very slightly, suggesting that both Li_2S deposition and polysulfide dissolution are inhibited. However, we again observe that the impedance behaviour of CMK-3/S/D[**14**] is better than CMK-3/D[**14**]/S.

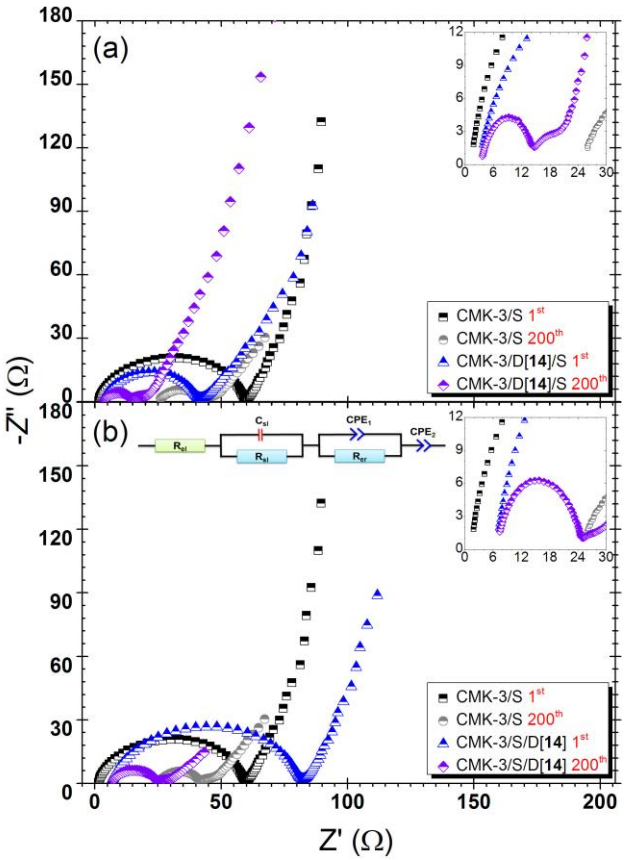

Figure 4 The Nyquist plots of (a). Comparison of CMK-3/D[**14**]/S at 1st and 200th cycle; and (d). Comparison of CMK-3/S/D[**14**] at 1st and 200th cycle. The EIS data of CMK-3/S without DNA modification were also included.

Finally, we employed the schemes displayed in Fig. 5 to elucidate underlying mechanism of the improved cyclic performance brought by DNA decoration. The as-expected improvement, for either pre-load or post-load strategy, is definitely ascribed to the anchoring function of the heteroatoms dispersed on the DNA strains towards lithium polysulfides. When DNA was loaded before S impregnation, the strains are randomly dispersed in the CMK-3 substrate and are mostly

besieged by S contents upon S impregnation, where DNA serves as octopus to grab polysulfides formed adjacently. Even if the DNA strains are not adjacent to the S content, the dissolved polysulfides may be recaptured by the free strains, leading to better capacity retention. Such a close encapsulation should has similar Ohmic resistance to the CMK-3/S electrode, however, the pre-load DNA strains in the CMK-3 substrate would make S particles more porous to facilitate electrolyte wetting (as evidenced by the BET data) and Li^+ transportation at electrode/electrolyte interface, leading to lower reaction impedance and more facile electrode reaction rate. In comparison, the high R_{er} of CMK-3/S should be the major reason that governs the relatively lower initial discharge capacity.

In contrast, for the post-load strategy, DNA would prefer to reside at the CMK-3/S interfaces around the open edges of the mesopores and serve as goal-keeper to prevent polysulfides from transporting from mesopores to electrolyte. Since DNA is insoluble in the electrolyte, the increased Ohmic resistance originates only from the electrode, which implies that the DNA strains should cover parts of the exposed CMK-3 surfaces. Due to the affinity of DNA to the ions in electrolyte, the post-loaded DNA strains locating at CMK-3/S boundary create more affinitive sites for electrolyte, which should enhance the surface wetting and lead to even lower surface layer impedance, however, the physically trapped ions around the DNA strains would apparently lower down the electrode reaction rate, as demonstrated by the increased electrode reaction impedance.

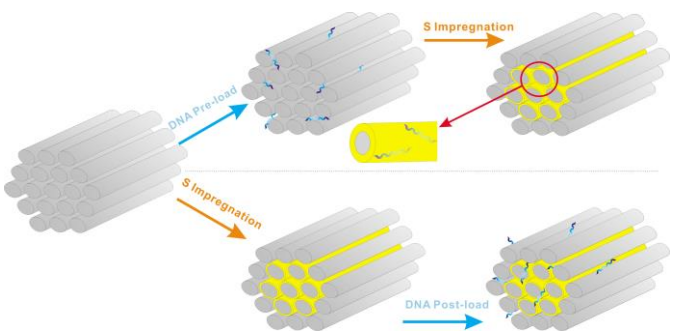

Figure 5. Illustration for the coexistence of CMK-3, S and DNA via pre- (upper part) and post-load (down part) of DNA.

The Coulombic Efficiency (CE) of the two selected test cells was depicted in Fig. S7. We note that the CE of CMK-3/S/D[**14**] fluctuates slightly around 80%, while that of CMK-3/D[**14**]/S increases with cycling and averages to be 83%. Although the first discharge capacity of CMK-3/D[**14**]/S is slightly higher than that of CMK-3/S/D[**14**], the latter one show a more smoother decaying trend than that of the formal one. Additionally, we also note that the pre-load procedure is more sensitive to the DNA loading amount (as seen in the discharge curves for CMK-3/D[**7**]/S and CMK-3/D[**22**]/S in Fig. 2(a) and 2(b)). Combining the above results, we can modestly deem that post-load procedure is more appropriate than pre-load strategy. For both the two loading sequences, a moderate DNA loading rate always gives the best performance, while low or high loading behave worse, however, still better than undecorated CMK-3/S electrode. Low loading, of course, provides less adsorption sites for polysulfides; while for high loading, although more adsorption sites are available, the self-aggregation of DNA might occur, leading to low adsorption efficiency.

Experimental

Synthesis of DNA decorated CMK-3/S composite

We first prepared different concentrations of aqueous DNA solution by dissolving certain amounts (10.5 mg, 21.0 mg, and 33.0 mg) of salmon sperm DNA powder (<50 bp, <17 nm, 99% purity, Biodee company) to 150 mL deionized water at 60 °C. The CMK-3 carbon (pore diameter is 3.6 nm, XFNANO Company, 1.0 g per time and used as received) was next ultrasonically dispersed into the solution at room temperature and stirred for 4 h at 80 °C. The mixture was slowly evaporated at 50 °C to ensure all DNA strains were uniformly absorbed by the CMK-3 substrate. The solid residue was dried in vacuum at 60 °C for 12 h (denoted by CMK-3/D). A typical melting-diffusion procedure was next employed to couple sulfur (Sinopharm Chemical Reagent Company, 99.9% purity, used as received) to the CMK-3/D substrate with a CMK-3/D: S weight ratio of 4:6 at 155 °C for 6 h in a tubular furnace under N_2 atmosphere[22]. Though CMK-3 always has the high sulfur loading rate even up to 70 wt%, the sulfur rate is about 60 wt% in our work to ensure enough space to the sulfur volume variation. Here, we used CMK-3/D/S to represent the product from the DNA pre-load procedure. Another strategy, named as DNA post-load procedure, was also carried out by changing the loading sequence of DNA and S with approximate loading rate. CMK-3 carbon was first prepared with S via exactly the same melting-diffusion method, followed by the dispersion-evaporation procedure to load the DNA strains, yielding the contrastive hybrid product denoted by CMK-3/S/D. For comparison, blank CMK-3/S sample was also prepared using the melting-diffusion method to evaluate the effect brought by DNA.

Material Characterizations

The structural and morphological features of the complexes were characterized via a Brunauer−Emmett−Teller (BET) method using nitrogen adsorption and desorption isotherms apparatus (ASAP2020 HD88, Micromeritics, USA), STEM (CM12, Philips, Netherlands) and SEM (Quanta200, FEI, USA), respectively, while the corresponding S contents in the complexes were determined by TGA-DSC (STA449 F3, NETZSCH, Germany) where the temperature range was set to be 30-600 °C with a heating rate of 10 °C·min^{-1} under N_2 atmosphere.

Cell Assembly and Electrochemical Test

We next grounded the obtained CMK-3/D/S, CMK-3/S/D and CMK-3/S powders with Super P conductive carbon and poly(vinylidene fluoride) binder with a weight ratio of 84:8:8. The mixture was dispersed into N-methyl-pyrrolidone (NMP) and slurry-cast onto aluminium current collector (the thickness is 200 μm). The punched cathodes are round shaped with a diameter and thickness of 15 mm and 0.1 mm respectively, where the net weight of active electrode material (C, S and PVDF) was measured to be around 8 mg (areal S uptake of ~2.13 mg·cm^{-2}). The cathodes were dried at 60 °C for 12 h in a vacuum oven before assembling to test cells. Here we employed 1 M LiTFSI in DOL/DME (volume ratio 1:1) as electrolyte (62.5 μL per cell) and lithium metal foil as the counter electrode. The separator was Celgard 2400 microporous membrane and the battery case was CR2025. Test cells were assembled in an Ar atmosphere at room temperature.

The electrochemical impedance spectroscopy analysis (EIS) test was carried out on a Bio-logic VMP3 (France), in which the amplitude and frequency range of EIS measurements were set to be 5 mV and 10^{5}–10^{-2} Hz respectively. The cyclic performance of the test cells were characterized on an Arbin tester (BT2000, USA) at different charge/discharge rate between 1.5 V and 3.0 V (vs. Li/Li^{+}).

Conclusions

In the present work, we selected the light-weighted and functional group abundant DNA as a third-party additive to decorate CMK-3 and S electrodes for purpose of improving the cyclic performance of Li/S cells. Our first-principles density functional theory calculations suggested that DNA was demonstrated to be capable of anchoring the most soluble Li_2S_8 via the constituent −P=O and =N− sites. Consequently, the polysulfides dissolution can be largely inhibited. From the experimental aspect, the DNA loading amounts as well as DNA loading sequences were optimized according to the test cell performances. With an S uptake of around 56 wt%, the existence of DNA or the loading sequences influences very slight to S loading or composite morphologies. For either DNA pre-load or post-load procedures, the cyclic performance depends on the DNA loading amount. A moderate DNA loading rate (14 $mg{\cdot}g^{-1}$ S, 0.83 wt% of total active components) gives the best cyclic performance for both pre- and post-load strategies. The post-load sample, CMK-3/S/D[**14**], hosts a discharge capacity of 771 $mAh{\cdot}g^{-1}$ at 0.1 C after 200 cycles and remains 70.7% of the initials, which behaves slightly better than the pre-load cases. By analysis the EIS data, we deduced that for pre-load, lower reaction impedance was gained, which makes the composite more porous to facilitate the electrolyte wetting; for post-load, similar tendency of Ohmic and reaction impedance are led by DNA strains locating at the CMK-3/S boundaries which create more affinitive sites for polysulfides. The significantly decreased electrolyte resistance in both CMK-3/D[**14**]/S and CMK-3/S/D[**14**] after 200^{th} cycles implies that a fine adding amount of DNA provides sufficient anchoring role and is capable of minimizing polysulfides dissolution. The DNA-decoration strategy for C/S electrodes can be facilely implemented in industry and provides a commercially feasible choice for pursuing high-performance lithium-sulfur batteries.

Acknowledgements

This work was supported by the Fundamental Research Founds for National University, China University of Geosciences Wuhan (Tengfei plan, Grant. CUG 110501; Innovative Team, Grant CUG120115), and the Natural Science Foundation of Hubei (Grant 2013CFB413 and 2011CDA070). The authors acknowledge Prof. Yaping Wang from Institute of Hydrobiology, China Academy of Sciences, and Dr. Xiaojun Kang from College of Computer Science, China University of Geosciences Wuhan, for helping purifying the DNA precursors.

Notes and references

[a] Sustainable Energy Laboratory, Faculty of Materials Science and Chemistry, China University of Geosciences Wuhan, Wuhan 430074, Hubei, China P.R.

[b] School of Environmental Studies, China University of Geosciences Wuhan, Wuhan 430074, Hubei, China P.R.

Email: cgzhou@cug.edu.cn (C.Z.); wujp@cug.edu.cn (J.W.)

Electronic Supplementary Information (ESI) available: The computational details, SEM images, TG-DSC measurement of the thermal stability of pure DNA and calculation for sulfur loading in different samples, BET results, Coulombic efficiency and fitted values for the equivalent circuit elements in EIS data are included. See DOI: 10.1039/b000000x/

1. A. Hayashi, T. Ohtomo, F. Mizuno, K. Tadanaga and M. Tatsumisago, *Electrochem. Commun.*, 2003, **5**, 701-705.
2. S. S. Jeong, Y. Lim, Y. J. Choi, G. B. Cho, K. W. Kim, H. J. Ahn and K. K. Cho, *J. Power Sources*, 2007, **174**, 745-750.
3. J. H. Yu, J. W. Park, Q. Wang, H. S. Ryu, K. W. Kim, J. H. Ahn, Y. Kang, G. Wang and H. J. Ahn, *Mater. Res. Bull.*, 2012, **47**, 2827-2829.
4. S. S. Zhang, *Electrochim. Acta*, 2012, **70**, 344-348.
5. M. Agostini, Y. Aihara, T. Yamada, B. Scrosati and J. Hassoun, *Solid State Ionics.*, 2013, **244**, 48-51.
6. M. Nagao, Y. Imade, H. Narisawa, T. Kobayashi, R. Watanabe, T. Yokoi, T. Tatsumi and R. Kanno, *J. Power Sources*, 2013, **222**, 237-242.
7. J. Guo, Y. Xu and C. Wang, *Nano Lett.*, 2011, **11**, 4288-4294.
8. J. J. Chen, Q. Zhang, Y. N. Shi, L. L. Qin, Y. Cao, M. S. Zheng and Q. F. Dong, *Phys. Chem. Chem. Phys.*, 2012, **14**, 5376-5382.
9. R. Chen, T. Zhao, J. Lu, F. Wu, L. Li, J. Chen, G. Tan, Y. Ye and K. Amine, *Nano Lett.*, 2013, **13**, 4642-4649.
10. K. Zhang, Z. Hu and J. Chen, *J. Energy Chem.*, 2013, **22**, 214-225.
11. Y. Cao, X. Li, I. A. Aksay, J. Lemmon, Z. Nie, Z. Yang and J. Liu, *Phys. Chem. Chem. Phys.*, 2011, **13**, 7660-7665.
12. L. Ji, M. Rao, H. Zheng, L. Zhang, Y. Li, W. Duan, J. Guo, E. J. Cairns and Y. Zhang, *J. Am. Chem. Soc.*, 2011, **133**, 18522-18525.
13. H. Wang, Y. Yang, Y. Liang, J. T. Robinson, Y. Li, A. Jackson, Y. Cui and H. Dai, *Nano Lett.*, 2011, **11**, 2644-2647.
14. S. Evers and L. F. Nazar, *Chem. Commun.*, 2012, **48**, 1233-1235.
15. B. Wang, K. Li, D. Su, H. Ahn and G. Wang, *Chem.-Asian J.*, 2012, **7**, 1637-1643.
16. Y. X. Wang, L. Huang, L. C. Sun, S. Y. Xie, G. L. Xu, S. R. Chen, Y. F. Xu, J. T. Li, S. L. Chou, S. X. Dou and S. G. Sun, *J. Mater. Chem.*, 2012, **22**, 4744-4750.
17. F. Zhang, X. Zhang, Y. Dong and L. Wang, *J. Mater. Chem.*, 2012, **22**, 11452-11454.
18. L. Zhang, L. Ji, P.-A. Glans, Y. Zhang, J. Zhu and J. Guo, *Phys. Chem. Chem. Phys.*, 2012, **14**, 13670-13675.
19. M. Q. Zhao, X. F. Liu, Q. Zhang, G. L. Tian, J. Q. Huang, W. Zhu and F. Wei, *ACS Nano*, 2012, **6**, 10759-10769.
20. C. Zhang, N. Mahmood, H. Yin, F. Liu and Y. Hou, *Adv. Mater.*, 2013, **25**, 4932-4937.
21. G. Zhou, L.-C. Yin, D.-W. Wang, L. Li, S. Pei, I. R. Gentle, F. Li and H.-M. Cheng, *ACS Nano*, 2013, **7**, 5367-5375.
22. X. Ji, K. T. Lee and L. F. Nazar, *Nat. Mater.*, 2009, **8**, 500-506.

23. B. Ding, C. Yuan, L. Shen, G. Xu, P. Nie and X. Zhang, *Chem. - Eur. J.*, 2013, **19**, 1013-1019.
24. F. Sun, J. Wang, H. Chen, W. Qiao, L. Ling and D. Long, *Sci. Rep.*, 2013, **3**, 2823.
25. N. Jayaprakash, J. Shen, S. S. Moganty, A. Corona and L. A. Archer, *Angew. Chem. Int. Ed.*, 2011, **50**, 5904-5908.
26. K. Zhang, Q. Zhao, Z. Tao and J. Chen, *Nano Res.*, 2013, **6**, 38-46.
27. G. Zheng, Y. Yang, J. J. Cha, S. S. Hong and Y. Cui, *Nano Lett.*, 2011, **11**, 4462-4467.
28. G. Zheng, Q. Zhang, J. J. Cha, Y. Yang, W. Li, Z. W. Seh and Y. Cui, *Nano Lett.*, 2013, **13**, 1265-1270.
29. B. Zhang, X. Qin, G. R. Li and X. P. Gao, *Energ. Environ. Sci.*, 2010, **3**, 1531-1537.
30. T. Xu, J. Song, M. L. Gordin, H. Sohn, Z. Yu, S. Chen and D. Wang, *ACS Appl. Mat. Interfaces*, 2013, **5**, 11355-11362.
31. Y. Fu and A. Manthiram, *Chem. Mater.*, 2012, **24**, 3081-3087.
32. J. Shao, X. Li, L. Zhang, Q. Qu and H. Zheng, *Nanoscale*, 2013, **5**, 1460-1464.
33. Y. Zhang, Y. Zhao, A. Konarov, D. Gosselink, Z. Li, M. Ghaznavi and P. Chen, *J. Nanopart. Res.*, 2013, **15**, 1-7.
34. W. Zhou, Y. Yu, H. Chen, F. J. DiSalvo and H. D. Abruna, *J. Am. Chem. Soc.*, 2013, **135**, 16736-16743.
35. G. Ma, Z. Wen, J. Jin, Y. Lu, X. Wu, M. Wu and C. Chen, *J. Mater. Chem. A*, 2014, **2**, 10350.
36. W. Li, G. Zheng, Y. Yang, Z. W. Seh, N. Liu and Y. Cui, *Proc. Natl. Acad. Sci. U. S. A.*, 2013, **110**, 7148-7153.
37. H. Chen, W. Dong, J. Ge, C. Wang, X. Wu, W. Lu and L. Chen, *Sci. Rep.*, 2013, **3**, 1910.
38. W. Li, Q. Zhang, G. Zheng, Z. W. Seh, H. Yao and Y. Cui, *Nano Lett.*, 2013, **13**, 5534-5540.
39. Y. Yang, G. Yu, J. J. Cha, H. Wu, M. Vosgueritchian, Y. Yao, Z. Bao and Y. Cui, *ACS Nano*, 2011, **5**, 9187-9193.
40. Y. Fu and A. Manthiram, *RSC Adv.*, 2012, **2**, 5927-5929.
41. Y. Fu, Y. S. Su and A. Manthiram, *ACS Appl. Mat. Interfaces*, 2012, **4**, 6046-6052.
42. G. C. Li, G. R. Li, S. H. Ye and X. P. Gao, *Adv. Eng. Mater.*, 2012, **2**, 1238-1245.
43. L. X. Miao, W. K. Wang, A. B. Wang, K. G. Yuan and Y. S. Yang, *J. Mater. Chem. A*, 2013, **1**, 11659-11664.
44. C. Wang, W. Wan, J. T. Chen, H. H. Zhou, X. X. Zhang, L. X. Yuan and Y. H. Huang, *J. Mater. Chem. A*, 2013, **1**, 1716-1723.
45. M. Wang, W. Wang, A. Wang, K. Yuan, L. Miao, X. Zhang, Y. Huang, Z. Yu and J. Qiu, *Chem. Commun.*, 2013, **49**, 10263-10265.
46. W. Zhou, H. Chen, Y. Yu, D. Wang, Z. Cui, F. J. DiSalvo and H. D. Abruna, *ACS Nano*, 2013, **7**, 8801-8808.
47. Q. Tang, Z. Shan, L. Wang, X. Qin, K. Zhu, J. Tian and X. Liu, *J. Power Sources*, 2014, **246**, 253-259.
48. G. Ma, Z. Wen, J. Jin, Y. Lu, K. Rui, X. Wu, M. Wu and J. Zhang, *J. Power Sources*, 2014, **254**, 353-359.
49. K. T. Lee, R. Black, T. Yim, X. Ji and L. F. Nazar, *Adv. Eng. Mater.*, 2012, **2**, 1490-1496.
50. Z. W. Seh, W. Li, J. J. Cha, G. Zheng, Y. Yang, M. T. McDowell, P.-C. Hsu and Y. Cui, *Nat. Comm.*, 2013, **4**, 1331.
51. X. Tao, F. Chen, Y. Xia, H. Huang, Y. Gan, X. Chen and W. Zhang, *Chem. Commun.*, 2013, **49**, 4513-4515.
52. Q. Pang, D. Kundu, M. Cuisinier and L. F. Nazar, *Nat. Comm.*, 2014, **5**, 4759.
53. J. X. Song, T. Xu, M. L. Gordin, P. Y. Zhu, D. P. Lv, Y. B. Jiang, Y. S. Chen, Y. H. Duan and D. H. Wang, *Adv. Funct. Mater.*, 2014, **24**, 1243-1250.
54. H. J. Peng, T. Z. Hou, Q. Zhang, J. Q. Huang, X. B. Cheng, M. Q. Guo, Z. Yuan, L. Y. He and F. Wei, *Adv. Mat. Interfaces*, 2014, **1**.
55. Z. W. Seh, Q. Zhang, W. Li, G. Zheng, H. Yao and Y. Cui, *Chem. Sci.*, 2013, **4**, 3673-3677.
56. M. Hagen, P. Schiffels, M. Hammer, S. Doerfler, J. Tuebke, M. J. Hoffmann, H. Althues and S. Kaskel, *J. Electrochem. Soc.*, 2013, **160**, A1205-A1214.
57. V. S. Kolosnitsyn, E. V. Kuzmina, E. V. Karaseva and S. E. Mochalov, *J. Power Sources*, 2011, **196**, 1478-1482.
58. V. S. Kolosnitsyn, E. V. Kuz'mina, E. V. Karaseva and S. E. Mochalov, *Russ. J. Electrochem.*, 2011, **47**, 793-798.